scientific reports

Check for updates

OPEN

Housing RCS rats under specific pathogen-free conditions mildly ameliorates retinal degeneration and alters intestine microbiota

Hadas Ketter-Katz[1,2,8], Rawan Saeed[1,2,8], Ifat Sher[1,2,3], Gali Altmann[1,2], Tal Shadi[1,2], Shada Dallasheh[1,2], Yael Lustig-Barzelay[1], Amit Sabo[1], George Jejelava[1,4], Rotem Hadar[5], Gilat Efroni[5], Amnon Amir[5], Tzipi Braun[5], Yael Haberman[5,6,8]✉ & Ygal Rotenstreich[1,2,7,8]✉

Retinitis pigmentosa (RP) is a genetic blinding disease with over 80 causative genes. Disease progression varies between patients with similar genetic backgrounds. We assessed the association between environment, gut microbiota, and retinal degeneration in the RP rat model Royal College of Surgeons (RCS). The rats were born and raised for two generations under specific pathogen-free (SPF, n = 69) or non-SPF conditions (n = 48). At the age of four weeks, SPF rats had significantly shorter dark-adapted a-wave and dark and light-adapted b-wave implicit times by electroretinogram ($p = 0.014$, $p = 9.5*10^{-6}$, $p = 0.009$, respectively). The SPF rats had significantly less photoreceptor apoptosis at ages four, eight, and twelve weeks (all $p < 0.022$), significantly thicker debris zone at age 14 weeks, and smaller hypofluorescent lesions in SPF rats at ages 10–16 weeks, especially in the inferior retina. The non-SPF rats had significantly higher microbiota alpha diversity ($p = 0.037$) and failed to present the age-related maturation of Proteobacteria, Spirochaetes, Actinobacteria, and Bacteroidetes seen in SPF conditions. Specific microbial amplicon sequence variants were reduced in rats with more severe retinal degeneration. Our data suggest an environmental effect on retinal deterioration in RCS rats. These findings may lead to the development of novel microbiome-related interventions for retinal degeneration.

Keywords Retinitis pigmentosa, Microbiome, RCS rats, Retinal degeneration, Photoreceptors

Retinitis pigmentosa (RP) is a blinding disease affecting 1:3000–1:4000 individuals[1]. It is caused by dysfunction and degeneration of retinal photoreceptor cells. RP patients typically lose their night vision first, followed by a gradual loss of peripheral vision. The disease is highly genetically heterogeneous, with 81 known causative genes and thousands of mutations identified[2]. Although the sequences of events (i.e., clinical manifestations) of the various sub-types of RP are well documented, this sequential progression varies from individual to individual. Even in patients with mutations in the same gene and gene region, disease course and onset time may vary considerably[3]. For example, in a study on disease progression in patients with mutations in the gene encoding the photosensitive protein rhodopsin (*RHO*), patients presented large intra-familial phenotypic variability and incomplete penetrance[1,3]. Furthermore, patients' age, sex, baseline retinal function, and affected gene region could account for less than a third of the variation in rates of change in retinal function in these patients[4]. Intervention studies further support the notion that factor(s) other than the genetic mutation, such as diet, epigenetic mechanisms, environmental and immunological conditions, may affect the clinical course of RP[5–8].

The human intestinal microbiota is key in promoting local and systemic immunity, processing energy and nutrients, and protecting cells from injury[9]. Dysbiosis or deviation from what is considered a healthy microbiota

[1]The Goldschleger Eye Institute, Sheba Medical Center, 5262100 Tel Hashomer, Israel. [2]Ophthalmology Department, Faculty of Medical and Health Sciences, Tel Aviv University, Tel Aviv, 6997801, Israel. [3]The Nehemia Rubin Excellence in Biomedical Research, TELEM Program, Sheba Medical Center, Tel Hashomer, 5262100, Israel. [4]The University of Pennsylvania, Philadelphia, PA 19104, USA. [5]Sheba Medical Center, Tel-Hashomer, affiliated with the Tel-Aviv University, Tel Aviv, Israel. [6]Cincinnati Children's Hospital Medical Center, The University of Cincinnati College of Medicine, Cincinnati, OH, USA. [7]Sagol School of Neuroscience, Tel Aviv University, Tel Aviv, 6997801, Israel. [8]These authors contributed equally: Hadas Ketter-Katz, Rawan Saeed, Yael Haberman and Ygal Rotenstreich. ✉email: Yael.Habermlan@sheba.health.gov.il; ygal.Rotenstreich@sheba.health.gov.il

may impair those vital functions. Geography[10], age[11,12], lifestyle[10], and medications[13] have all been associated with the gut microbiome composition. Previous studies have demonstrated that environmental factors, not genetics, predominantly shape the composition of the gut microbiome[14]. Microbial composition significantly affected local central nervous system (CNS) inflammation and neurodegenerative diseases[15–19]. Recent studies indicated a possible link between the gut and oral microbiome and neurodegenerative ocular pathologies, including glaucoma and age-related macular degeneration (AMD)[20,21].

In 1962, specific-pathogen-free (SPF) housing conditions were introduced by the National Institute of Health (NIH) to minimize infections and diseases in laboratory rodents and to assist in standardizing study results[22]. Recent studies indicated that SPF housing leads not only to alternations in gut microbiome but also to broad changes in the immune system, influencing animal's metabolism, general physiology, and even the circadian rhythm[22–25]. Some of these physiological changes could be reversed by returning the rodents to a conventional non-SPF facility[22–25].

This study aimed to determine the associations between gut microbiome and photoreceptor degeneration in Royal College Surgeon (RCS) rats, a widely-used rodent model for RP. These rats carry a deletion mutation in the *MERTK* gene, which attenuates photoreceptor outer segment (POS) phagocytosis by retinal pigment epithelium (RPE) cells, leading to the accumulation of POS in a subretinal layer known as the debris zone (DZ), and gradual degeneration of photoreceptor cells[26,27]. Our results indicate slower photoreceptor degeneration in RCS rats reared under SPF conditions than in non-SPF conditions, which was associated with alterations in microbial composition, suggesting a protective influence of the environment on the retina in a rodent model of RP.

Results

Characterization of retinal function and structure in RCS and Long–Evans (WT) rats

To assess the association of microbiome diversity and retinal degeneration, we first compared the retinal structure and function between RCS rats (n = 69) and their WT *Long–Evans* counterparts ("WT" rats, n = 26) born and raised in an SPF facility at various ages.

As expected, RCS rats presented with significantly lower mean dark-adapted a-wave compared to WT rats at the age of four weeks (mean ± standard error, SE: 40.1 µV ± 7.3 µV vs. 317.9 µV ± 38.5 µV, $p = 0.000004$, Supplementary Fig. 1A). The mean maximal dark- and light-adapted ERG b-waves were also significantly lower compared to WT rats at the age of 4 weeks (232.7 µV ± 35.7 µV vs. 1695.2 µV ± 196.3 µV, $p = 0.0000028$; 128.1 µV ± 19.2 µV vs. 406.6 µV ± 49.2 µV, $p = 0.0001$, respectively, Supplementary Fig. 1B,C). As expected, the light-adapted ERG a-wave was undetectable in both species[28]. ERG responses were undetectable when RCS rats reached the age of 10 weeks old.

SD-OCT imaging indicated similar thickness of the photoreceptor nuclei layer (outer nuclear layer, ONL) in RCS and WT rats at the age of four weeks. The ONL layer was unmeasurable by SD-OCT in RCS rats by the age of 10 weeks. By contrast, in 10-week-old WT rats, the SD-OCT ONL thickness ranged between 69.6 µm at the mid-superior retina and 73.84 µm at the inferior retina (Supplementary Fig. 2).

Blue auto fluorescence fundus (BL-FAF) imaging analysis demonstrated intact fundus in WT rats up to 48 weeks. By contrast, at the age of 10 weeks, hypofluorescent foci, which are associated with the loss of photoreceptors and the thinning of the debris zone (DZ) layer[29], started to appear in RCS rats. By 16 weeks, the hypofluorescent area covered 7.71% of the superior and 5.39% of the inferior retina (Supplementary Fig. 3).

Analysis of microbiota composition in RCS and WT rats

To visualize the similarities and variations between the microbial composition in RCS versus WT rats, an unweighted UniFrac-based PCoA of the cohort was performed with a strong clustering separation between the rat strains, mostly on PC1 (Supplementary Fig. 4A). To quantify the contribution of different factors affecting the gut microbial composition, we used a PERMANOVA test (Supplementary Fig. 4B and Supplementary Database S1). PERMANOVA was applied while controlling for age (except when checking for age). Litter explained the greatest microbial variance (32%), followed by species (RCS vs. WT, 7%), and then by age (3%), SPF versus non-SPF (3%), and sex (2%). WT rats had significantly reduced alpha diversity (Faith's phylogenetic diversity, reflecting the intra-sample diversity, Supplementary Fig. 4C), with 681 significant differential abundant bacterial Amplicon sequence variants (ASVs) between RCS and WT (Supplementary Fig. 4D and Supplementary Database S1). Altogether, these data indicate substantial species-specific differences between WT and RCS rats.

Characterization of retinal structure in RCS rats raised under SPF versus non-SPF conditions by SD-OCT and BL-FAF imaging

Next, we characterized similarities and differences between RCS rats born and reared for two generations in SPF versus non-SPF conditions. As detailed in the "methods" section, similar light conditions were maintained in both facilities. Quantification of BL-FAF hypofluorescence revealed that RCS rats born and bred under SPF conditions presented smaller BL-FAF hypofluorescent areas in the superior retina compared to RCS rats born and reared in SPF conditions starting at the age of 12 weeks (mean ± SE: 2.51% ± 0.53% vs. 9.75% ± 3.06%, $p = 0.037$), and in the inferior retina at the ages ten weeks (1.71% ± 0.32% vs. 4.87% ± 1.83%, $p = 0.02$), 12 weeks (2.39% ± 0.79% vs. 15.26% ± 4.94%, $p = 0.003$), 14 weeks (3.72% ± 1.05% vs. 22.33% ± 6.38%, $p = 0.005$), and 16 weeks (5.77% ± 0.65% vs. 16.26% ± 3.47%, $p = 0.017$, Fig. 1).

To further characterize the effect of rearing the rats under SPF versus non-SPF conditions on retinal structure, SD-OCT imaging was performed, and the thicknesses of the total retina (TR), ONL, and DZ layers were determined every two weeks in the superior and inferior retina of each animal. Similar to previous publications[29,30], the total retina thickness decreased with age, with a thinner total retina in the inferior retina compared to the superior retina in all time points ($p = 1^{*}10^{-5}$, data not shown).

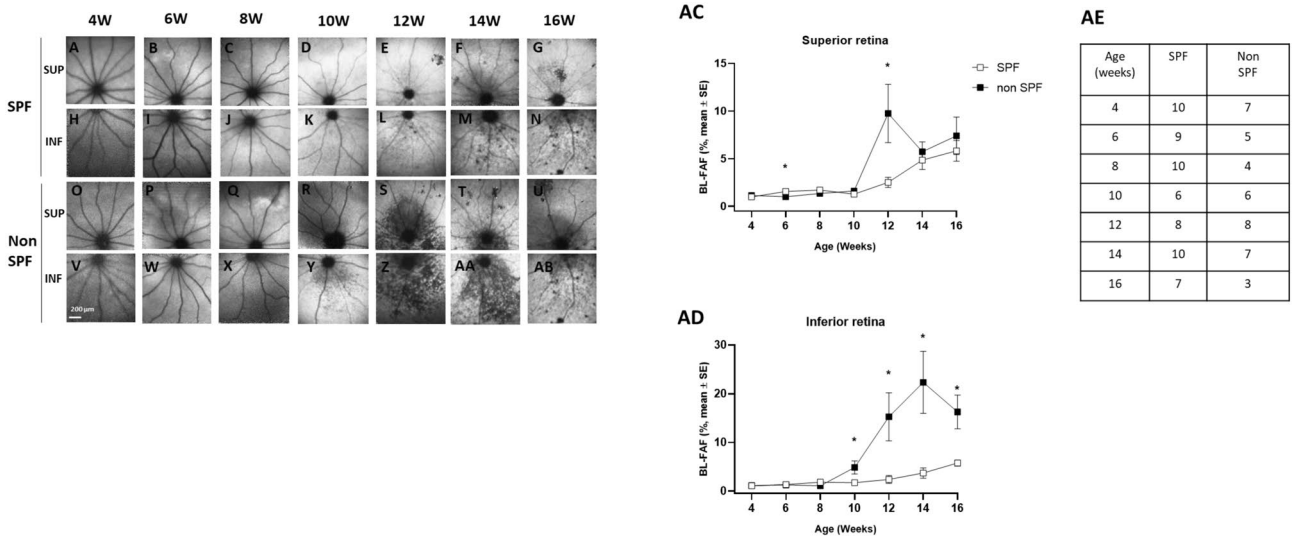

Age (weeks)	SPF	Non SPF
4	10	7
6	9	5
8	10	4
10	6	6
12	8	8
14	10	7
16	7	3

Fig. 1. BL-FAF imaging in RCS rats born and reared in SPF versus non-SPF conditions. **A–N:** Representative BL-FAF images of the superior (sup, **A**–**G**) and inferior (inf, H–N) retina of RCS rats born and reared for two generations in SPF conditions at the ages of 4 (**A**, **H**), 6 (**B**, **I**), 8 (**C, J**), 10 (**D**, **K**), 12 (**E**, **L**), 14 (**F**, **M**) and 16 weeks (**G**, **N**). **O-AB:** Representative BL-FAF images of the superior (**O**–**U**) and inferior (**V**–**AB**) retina of RCS rats born and reared in non-SPF conditions at the ages of 4 (**O**, **V**), 6 (**P**, **W**), 8 (**Q**, **X**), 10 (**R**, **Y**), 12 (**S**, **Z**), 14 (**T**, **AA**) and 16 weeks (**U**, **AB**). **AC–AD:** quantification of the BL-FAF hypofluorescent area in the superior (**AC**) and inferior retina (**AD**) demonstrates significantly larger BL-FAF hypofluorescent area in RCS rats born and raised in non-SPF conditions compared to RCS rats born and reared in SPF conditions at ages ≥ 10 weeks. Data are presented as mean ± SE. * denotes $p<0.05$. **AE:** The table depicts the number of RCS rats tested by BL-FAF imaging at each time point.

However, no significant differences were observed in the SD-OCT thickness of the total retina and ONL between SPF and non-SPF conditions (all $p > 0.051$ and $p > 0.283$, respectively, Supplementary Fig. 5). A significantly thicker SD-OCT DZ was measured in the SPF rats compared with non-SPF rats in the mid-inferior retina at the age of 14 weeks (32.4 µm ± 1.2 µm vs. 25.2µm ± 0.6µm, $p = 0.0003$, Supplementary Fig. 5G). A thicker SD-OCT DZ in the mid-inferior retina was also measured in the SPF rats at 12 weeks. Still, this difference did not reach statistical significance (36.1µm ± 2.4µm vs. 32.2µm ± 1.4µm, $p = 0.18$, Supplementary Fig. 5G).

Characterization of retinal function in RCS rats raised under SPF versus non-SPF conditions by ERG

Next, we assessed the effect of housing conditions on retinal function by ERG. Similar mean a- and b-wave amplitudes were recorded under dark adaption, and similar b-wave amplitudes were recorded under light adaptation conditions in SPF and non-SPF groups (all $p > 0.088$, $p>0.208$, and $p > 0.315$, respectively). However, as shown in Fig. 2, significantly shorter implicit time was recorded in rats born and reared in SPF conditions compared to non-SPF conditions at the age of four weeks for dark-adapted a-wave (mean ± SE: 19.85 ms ± 0.57 ms vs. 23.55 ms ± 1.27 ms, $p = 0.014$), dark-adapted b-wave (86.53 ms ± 4.13 ms vs. 115.54 ms ± 3.45 ms, $p=9.5 \times 10^{-6}$), and light-adapted b-wave (73.64 ms ± 4.47 ms vs. 93.27 ms ± 2.45 ms, $p = 0.009$). Representative ERG traces are shown in Supplementary Fig. 6.

Characterization of photoreceptor apoptosis and retinal structure by histology in RCS rats raised under SPF versus non-SPF conditions

Loss of photoreceptor cell bodies in the ONL is a primary characteristic of retinal degeneration in RCS rats, with apoptosis being a dominant mechanism of photoreceptor cell loss[29,31,32]. To assess the environmental effect on photoreceptor apoptosis, the number of TUNEL-positive nuclei in the ONL across the entire retinal section was determined. A lower number of photoreceptor cells was positive for TUNEL labeling in rats reared in SPF compared with non-SPF conditions at ages 4–12 weeks (ANOVA $p = 0.001$, Fig. 3). Pair-wise analysis indicated a significantly lower number of apoptotic photoreceptors in SPF-raised rats compared to non-SPF conditions at ages four weeks (mean ± standard deviation: 6.6 ± 1.3 vs.13.6 ± 1.7 TUNEL positive cells in the ONL/100µm retina, $p = 0.012$, Fig. 3A,F,K), eight weeks (12.3 ± 3.9 vs. 22.4 ± 4.1 TUNEL positive cells in the ONL/100µm retina, $p = 0.022$, n = 5 each group, Fig. 3C,H,K), and twelve weeks (8.5 ± 1.1 vs. 14.6 ± 2.1 TUNEL positive cells in the ONL/100µm retina, $p = 0.004$, Fig. 3E,J,K). To further assess the effect of housing conditions on photoreceptor degeneration, retinal sections were analyzed for ONL thickness by DAPI staining. At the age of four weeks, the ONL of the SPF group contained more cell layers compared with the non-SPF group (mean cell layers ± SE: 8.3 ± 0.36 cells vs. 6.9 ± 1.1 cells), but the difference was not significant ($p = 0.263$). No significant differences in the mean number of nuclear layers between the two groups were observed at later time points (Supplementary Fig. 7, all $p > 0.175$). In the rat retina, rods constitute the vast majority of photoreceptors, and cones degenerate slower than rods in the RCS rats[33]. Thus, the thinning of the ONL thickness mainly reflects the degeneration of

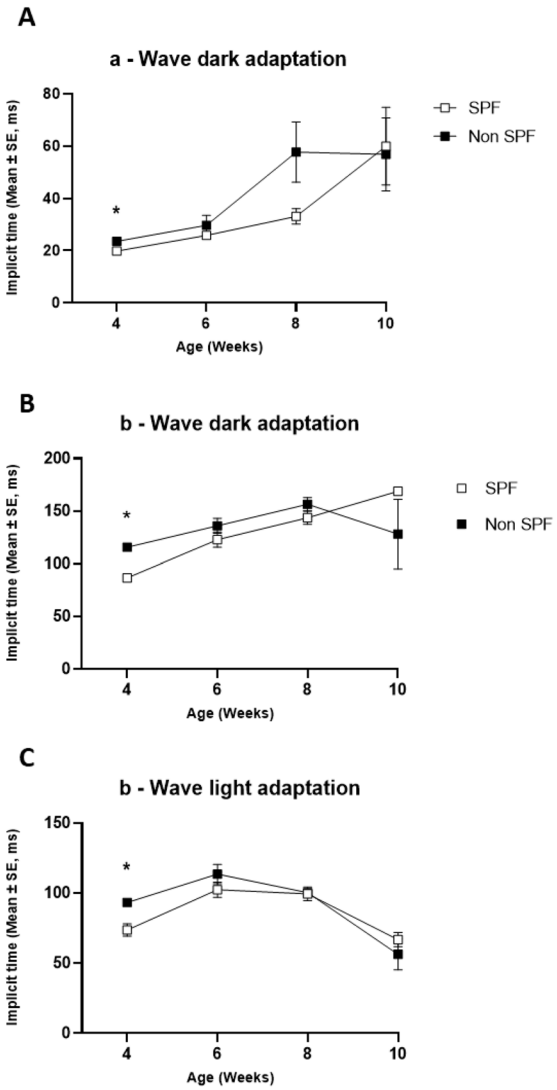

D

Age (weeks)	SPF	Non SPF
4	8	8
6	11	6
8	8	6
10	4	4

Fig. 2. Mean ERG implicit time in RCS rats born and reared under SPF versus non-SPF conditions. ERG implicit time was measured from light onset to maximal a-wave peak (**A**) and b-wave peak (**B**, **C**) under dark (**A** and **B**) and light (**C**) adaptation conditions. Data are presented as mean ± SE. Error bars not seen in the graph are smaller than 4.47 μV. * denotes $p<0.05$. (**D**) The table depicts the number of animals tested in each group at each time point.

rods. To assess the effect of housing conditions on cone degeneration, we performed an immunofluorescence analysis with antibodies directed against M/L-opsin and S-opsin. Asimilar cone cell density was identified in the SPF and non-SPF groups at various ages (data not shown).

The effect of housing conditions on gut microbiota

To assess the impact of the housing environment on rats' general health, rats were monitored for changes in weight between the ages of 4–16 weeks. No significant differences were observed between the SPF and non-SPF groups at ages 4–16 weeks (all $p > 0.06$, Supplementary Fig. 8).

Next, we tested for differences in the gut microbial composition between RCS rats born and reared under SPF (n = 46) vs. non-SPF (n = 41) conditions. An unweighted UniFrac-based PCoA colored by SPF and non-SPF conditions with some clustering separation is shown (Fig. 4A). SPF and non-SPF values significantly differed on PC2 (Wilcoxon p-value = 0.027). Coloring the samples by Rats' age also indicated interesting clustering, where most younger rats clustered on the top on PC2 (spearman correlation p-value = 2.3e-7, between PC2 and age, Fig. 4B). To quantify the contribution of different factors affecting the gut microbial composition, we used a PERMANOVA test (Fig. 4C and Supplementary Database S2). PERMANOVA was applied after controlling for age (except when checking for age, Fig. 4D). Litter explained the most significant variance (32%), followed by age (3.7%), retinal structure measurements, SPF versus non-SPF, and sex, each significantly explaining 1–3.2%

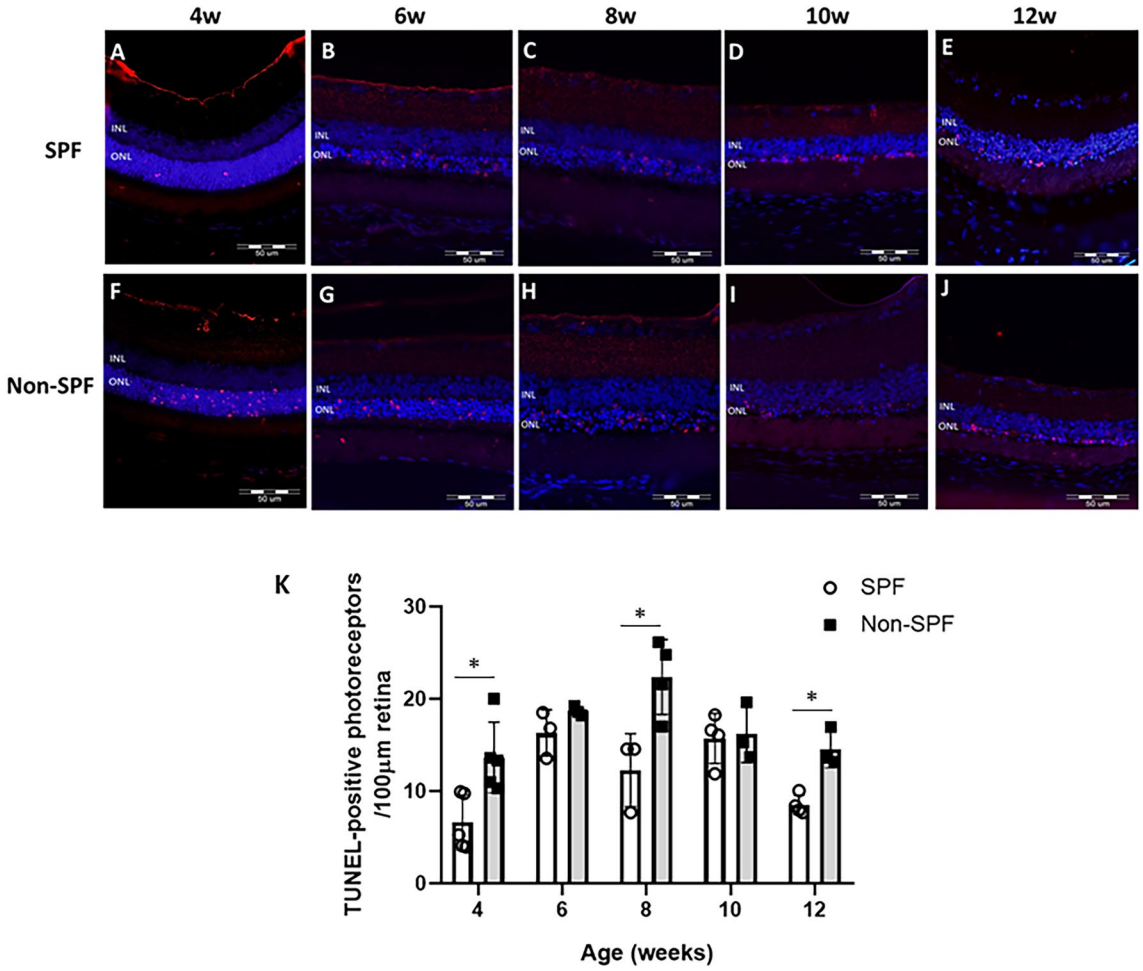

Fig. 3. Lower TUNEL labeling in ONL of RCS rats reared in SPF versus non-SPF conditions. Representative images of TUNEL-labeled retinal cross sections of rats raised under SPF or non-SPF conditions at indicated ages in weeks (w). Scale bar: 50 µm. ONL—outer nuclear layer, INL—inner nuclear layer. **K**- Quantification of TUNEL-positive nuclei in the ONL per 100 µm retina. The analysis included three to five rats in each group and two litters in each group, except the SPF group at week eight and the non-SPF group at week 10, which included three rats from a single litter.

of the microbial variations. Our analysis included 46 rats from 15 litters in the non-SPF group and 41 in the SPF group from 7 litters. PCA analysis indicated that the effect was not driven by a single litter Supplementary Fig. 9).

We further looked at age variation at the phyla level; we noted an age-related maturation with a significant increase in Proteobacteria and Spirochaetes and a decrease in Actinobacteria and Bacteroidetes in rats raised in SPF condition, while no significant phyla change was noted in non-SPF conditions when plotted against age. SPF rats had significantly reduced alpha diversity (Faith's phylogenetic diversity, Fig. 4E, Mann Whitney 2-sided $p < 0.05$), and 48 significant differential abundant bacterial ASVs were identified between SPF and non-SPF conditions (Fig. 4F and Supplementary Database S2).

To assess for specific associations between microbial ASVs and retinal function and structure, we used Maaslin2 (Multivariate Association with Linear Models). This multivariate analysis enables including and controlling for litter, sex, age, and SPF vs non-SPF in one model. These factors were included as they explained the highest and most significant microbial variation in the PERMANOVA test (Fig. 4C and Supplementary Datbase S2). We tested for a significant association of microbial ASVs with retinal function (represented by dark-adapted-b wave implicit time) and structure (BL-FAF hypofluorescent area in the inferior retina, "BL-FAF-inf") in the model. For the BL-FAF hypofluorescent area, animals were given a score of mild degeneration if the hypofluorescent area was ≤ 10% and "severe" if the hypofluorescent area was > 10%. Overall, several ASVs were correlated with age (Fig. 5A and Supplementary Databse S3) and SPF vs non-SPF (Fig. 5D). Four unique ASVs were significantly lower in rats with an inferior BL-FAF hypofluorescent area higher than 10% (Fig. 5Bi–iv). The four ASVs were Prevotella copri (ASV03122, $p = 7.10E{-}05$, q = 0.02, Fig. 5Bi), Ruminococcaceae Oscillospira (ASV12750, $p = 5.31E{-}05$, q = 0.021, Fig. 5Bii), Clostridia Clostridiales (ASV09046, $p = 2.35E{-}08$, q = 4.08E-05, Fig. 5Biii), and Clostridiales Lachnospiraceae (ASV09386, $p = 8.57E{-}07$, q = 0.0007, Fig. 5Biv). One ASV that showed significant increasing abundance with increasing rat age also showed a negative correlation with the dark-adapted-ERG b wave implicit time (Clostridia Clostridiales ASV10195, Fig. 5Ci, ii).

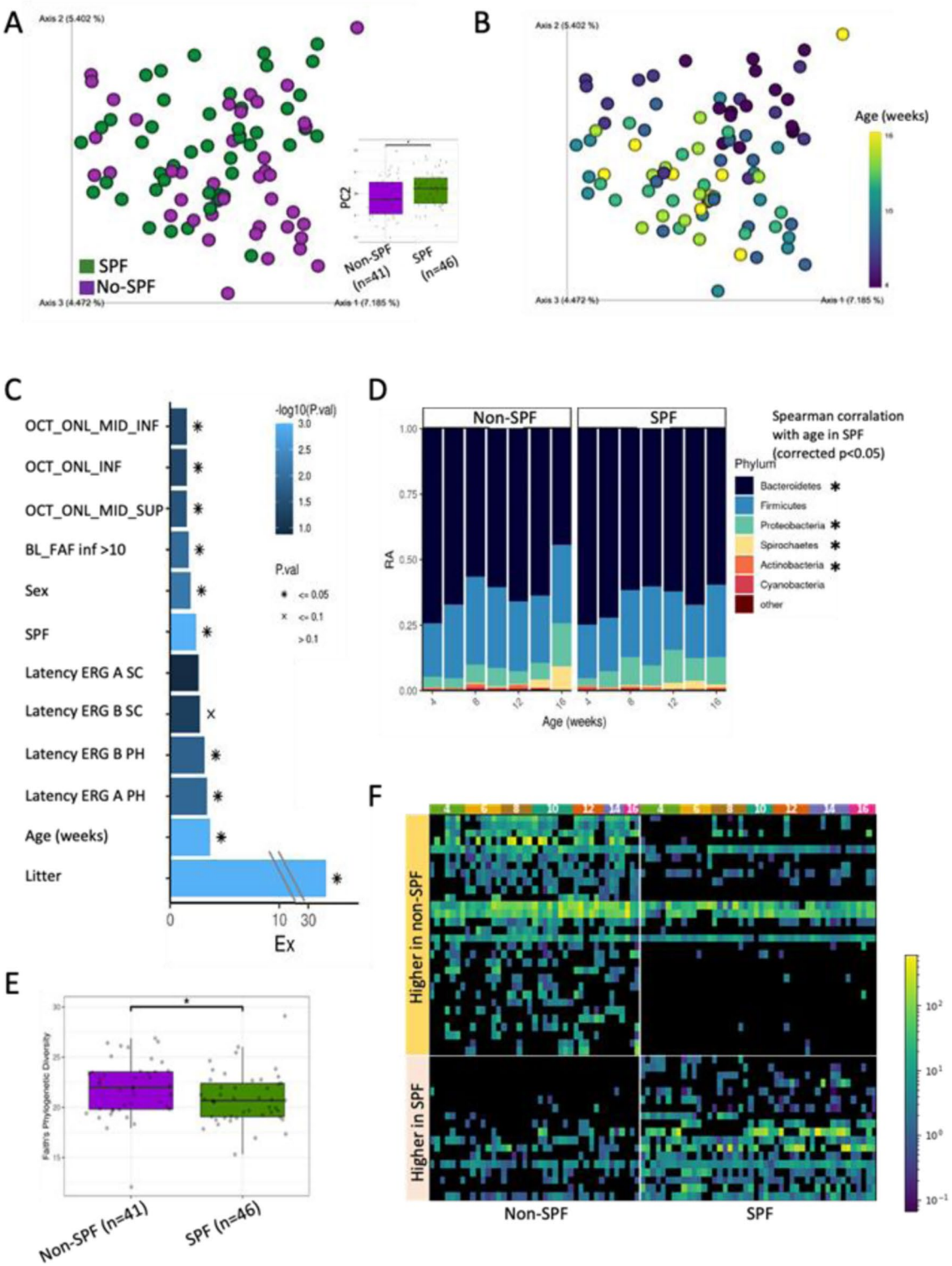

Discussion

The environment dominates over host genetics in shaping the gut microbiome[14]. Ocular diseases were already suggested to be affected by the gut–eye axis[34], namely the mutual interplay between the eye and the gut bacteria. The causal relationship between gut microbiota alterations and eye disease remains to be fully elucidated, but it has been hypothesized that microbial alterations in the gut may trigger a systemic inflammatory response and oxidative stress, which could contribute to retinal damage and eye disease progression. Murine RP models have a defined genetic background and are kept in a controlled and diverse environment thus offering the opportunity to evaluate associations observed in human patients and on disease progression more mechanistically. Here, we hypothesize that RP disease progression in the models will be associated with environmental exposures and alternations in the gut microbiome. Here, we demonstrate that degenerative changes in retinal function and structure

◂**Fig. 4.** Microbial composition of RCS rats reared under SPF and non-SPF conditions. Unweighted UniFrac PCoA plot representing RCS rats colored by rearing conditions (**A**) or age (**B**) with indicated PC1 and PC2, explaining 7.2% and 5.4% of the overall variation. SPF and non-SPF values significantly differed on PC2 (Wilcoxon p-value = 0.027), and there was a significant correlation between PC1 and age (spearman correlation p-value = 2.3e−7). (**C**) PERMANOVA shows that litter explained the greatest amount of variance (32%), followed by age (3.7%), and then by retinal function measurements (ERG implicit time). SPF vs non-SPF and sex significantly explained 1–3.2% of the microbial variations. * denotes $p \leq 0.05$). The variance was estimated for each feature independently while accounting for age. OCT_ONL_MID_INF = ONL thickness in the mid-inferior retina by SD-OCT (as presented in Supplementary Fig. 2); OCT_ONL_INF = ONL thickness in the inferior retina by SD-OCT; OCT_ONL_MID_SUP = ONL thickness in the mid-superior retina by SD-OCT. BL_FAF > 10 = blue fundus auto-fluorescent area in the inferior retina larger than 10%; SPF = Specific Pathogen Free; ERG_A_SC = ERG a-wave implicit time under dark adaptation (scotopic conditions); ERG_B_SC = ERG b-wave implicit time under dark adaptation (scotopic conditions); ERG_B_PH = ERG b-wave implicit time under light adaptation (photopic conditions); ERG_A_PH = ERG a-wave implicit time under light adaptation (photopic conditions). (**D**) Taxa bar plot indicating phylum level distribution by age is shown for SPF and non-SPF rats. * indicates age-related maturation with a significant increase (Spearman $p < 0.05$) in Proteobacteria and Spirochaetes and a decrease in Actinobacteria and Bacteroidetes in rats raised in SPF condition, while no significant phyla change was noted under non-SPF conditions. (**E**) Alpha diversity (Faith's phylogenetic diversity) plotted by rearing conditions (SPF vs. non-SPF), Mann Whitney, * denote $p < 0.05$. (**F**) Differential abundance (dsFDR < 0.05) between RCS rats reared under SPF and non-SPF conditions resulted in 48 amplicon sequence variants (ASVs), and those are shown as a heat-map (30 ASVs higher in non-SPF and 18 higher in SPF, see also Supplementary Database S2). The heat map indicates the relative abundance of each bacterial ASV in rows and different animal groups in columns, as indicated under the heat map. Each column represents an individual animal, and each row represents a different bacterial ASV. Relative frequency (shown on the right-hand color scale) is out of 10^4 normalized reads per sample. The list of ASVs and their taxonomy is presented in Supplementary Database S2.

concur with changes in growth environment and with shifts in gut microbiome composition in an animal model of RP. Rats born and reared under SPF conditions had significantly lower rates of photoreceptor apoptosis at ages four, eight, and 12 weeks, shorter ERG implicit time at age of four weeks, a thicker DZ in the mid inferior retina at the age of 14 weeks and a smaller BL-FAF hypofluorescent area at the ages of 10–16 weeks compared to RCS rats born and reared for two generations in non-SPF conditions. Interestingly, these differences were associated with changes in the overall gut microbial composition (48 ASVs were different in RCS rats grown in SPF vs non-SPF conditions), increased alpha-diversity in non-SPF versus SPF conditions, and a more organized microbial maturation with an increase in specific phyla seen more specifically under SPF conditions. Moreover, in a multivariate Maaslin model, we could link specific ASVs with retinal function and structure after controlling for other significant factors such as litter, age, sex, and rearing conditions (SPF/non-SPF). These findings suggest a link between environmental conditions, microbial composition, retinal function, and structure deterioration in genetically susceptible RCS rats.

BL-FAF imaging was used to assess retinal degeneration in vivo. As shown previously, retinal degeneration in RCS rats begins with the accumulation of debris in the photoreceptor outer segments. The debris zone layer is reflected in BL-FAF imaging as a hyperfluorescent signal throughout the posterior pole. This hyperfluorescent signal is gradually replaced by hypofluorescent areas as photoreceptor degenerate[29]. Our data indicates a significant association between the inferior BL-FAF signal and the overall microbial variation using PERMANOVA and with specific ASVs using a multivariate model including lower abundance of Prevotella copri (ASV03122), Ruminococcaceae Oscillospira (ASV12750), Clostridia Clostridiales (ASV09046), and Clostridiales Lachnospiraceae (ASV09386), in RCS rats with larger BL-FAF hypofluorescent area (above 10%).

Measurements of the time component in ERG (implicit time) reflect the general physiological health of photoreceptors[35–37]. The a-wave implicit time reflects the physiological response time of the photoreceptors in the outer retina. The b-wave implicit time reflects the physiological response time of the inner layers of the retina[38]. Delayed implicit time was recorded in RP patients, and the extent of implicit time delay is considered a good prognostic marker for disease progression[39]. Several studies reported increased scotopic a-wave implicit time in RCS rats aged four to ten weeks[40,41]. Ciavatta et al. reported that subretinal electrical stimulation treatment reduced the implicit time of both the a-wave and b-wave while enhancing the maximal amplitude of these waves following treatment[42]. In our study, although SPF and non-SPF rats did not differ in ERG amplitudes, significantly shorter a- and b-waves implicit time was recorded in young rats (age four weeks) born and reared for two generations in SPF conditions, suggesting a mild increase in the function of photoreceptors and inner retina layers compared to rats born and reared in non-SPF conditions at early stages of the disease. Furthermore, we show that at this young age, rats reared in SPF conditions presented with lower apoptosis rates in the photoreceptor layer and that the a-wave and b-wave implicit time was significantly associated with the overall microbial variation using PERMANOVA. Clostridia Clostridiales (ASV10195), which showed significant increasing abundance with increasing rat age, also negatively correlated with the dark-adapted-b wave implicit time, suggesting a link between environmental microbiome changes and retinal structure and function. Although the effect of housing conditions on retinal structure and function was mild, as no significant differences were observed in ERG amplitudes and ONL thickness, our data suggest a possible link between housing conditions, gut microbiome, and retinal degeneration, which may open the door for future microbiome manipulation as a potential strategy to slow down disease progression. The association between microbiome and retinal degeneration in humans, where disease progression is slower, remains to be determined.

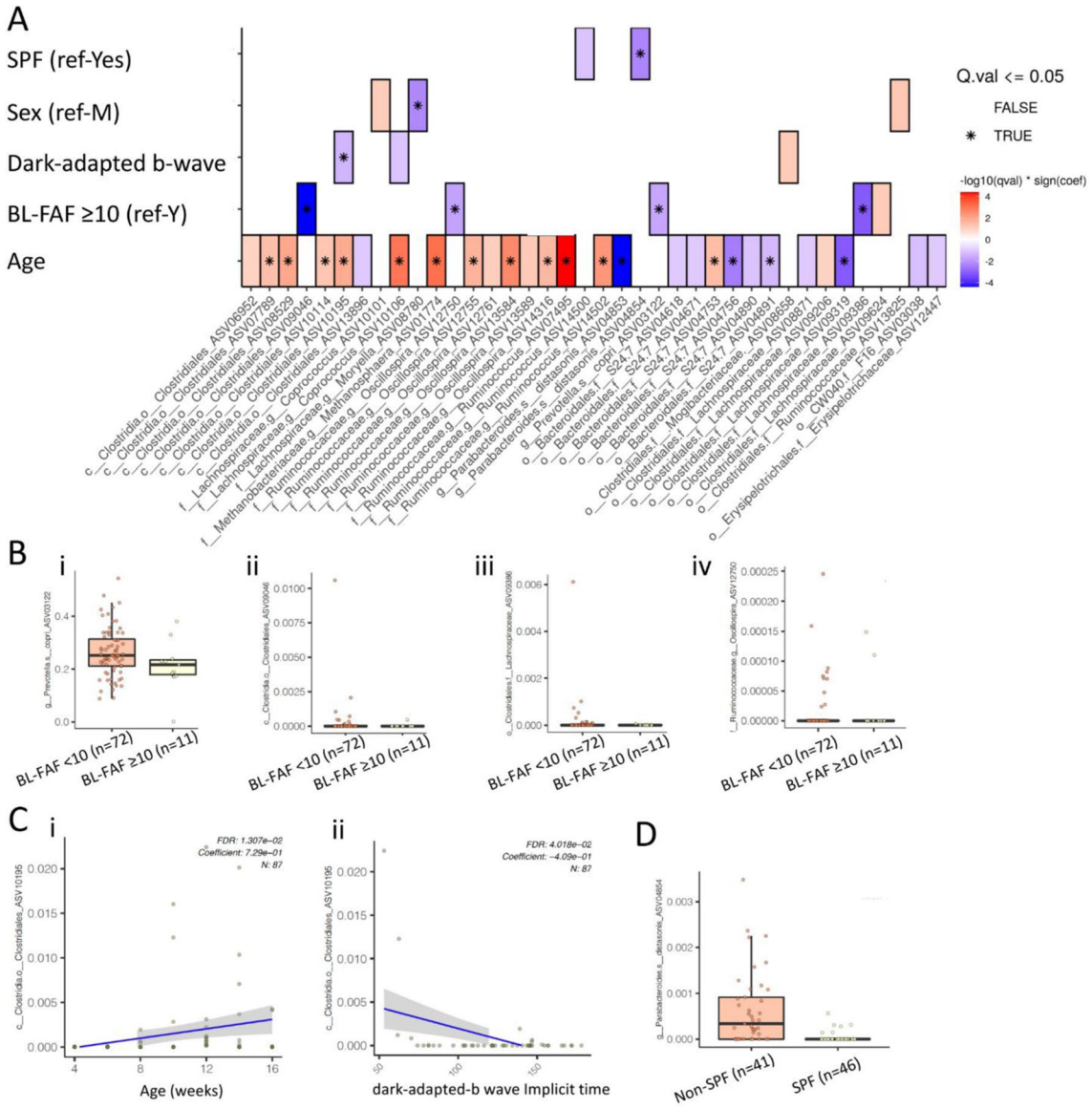

Fig. 5. Microbial taxa linked with retinal structure and function. (**A**) Multivariate association with linear models (Maaslin) was applied to associate between microbial abundance, dark-adapted ERG b wave implicit time and BL-FAF hypofluorescent area, after controlling for litter, age, sex, and rearing conditions (SPF/non-SPF). Taxonomic classification of the numbered ASV is indicated. The heat map indicates associations with $q < 0.1$, and the asterisks indicate associations with $q < 0.05$. The red color indicates positive and blue indicates negative association with continuous values, and increased or decreased (respectively) from the reference value (ref) in the case of dichotomous conditions (i.e., if the reference was male (M), red indicates higher in male and blue lower in male). (**B**) Specific associations of significant ASVs (from panel **A**) with BL-FAF hypofluorescent area in the inferior retina (**Bi–iv**, n = 83 samples), age (**Ci**), dark-adapted ERG b wave implicit time (**Cii**), and housing condition (**D**) are shown.

The retinal structure and function measures of RCS rats born and reared in non-SPF conditions reported here agree with the previously reported measurements for these animals in our lab and by other groups[43–47]. Surprisingly, although the photoreceptor apoptosis rate was nearly two-fold lower in the SPF group at ages four, eight, and twelve weeks, no significant differences were observed in ONL thickness by OCT or histology analysis. Apoptosis is considered a leading cause of photoreceptor degeneration in these rats[48]. Although no significant differences were observed in ONL thickness between SPF and non-SPF RCS rats, BL-FAF imaging revealed significantly smaller hypofluorescent lesions in the SPF compared with non-SPF rats at ages 10–16 weeks, corresponding with a thicker DZ layer in the SPF group at ages 14 and 16 weeks, especially in the inferior retina. Our previous studies indicated that the hypofluorescent spots spread in the RCS rats from the inferior retina to the nasal and temporal regions and reflected the loss of photoreceptors that resulted in a thinner DZ and lower accumulation of bis-retinoids and lipofuscin[29]. Our data suggest a mild amelioration of photoreceptor loss under SPF conditions.

Our findings that microbiome alterations are associated with retinal degeneration are in agreement with the recent study by Kutsyr et al., who reported an association between the decline in retinal function and photoreceptor degeneration and microbial gut dysbiosis as well as differences in alpha and beta diversity, and the microbial ASV levels in another rodent model of retinitis pigmentosa, the rd10 mice[49,50]. Patients with glaucoma present higher bacterial oral counts compared to control subjects[51,52]. Furthermore, subcutaneous lipopolysaccharide administration enhanced optic nerve degeneration, microglial activation in the optic nerve and retina, and up-regulation of toll-like receptor 4 (TLR4) and complement pathways in mice[53] .Pharmacologic blockade of TLR4 partially ameliorated the enhanced damage, suggesting that an increase in oral bacterial count may lead to neurodegeneration of the optic nerve via activation of microglia in the retina and optic nerve. Studies in wild-type mice demonstrated that a high-glycemic-index diet altered the gut microbiota and the production of metabolites, leading to age-related features of AMD, including outer and inner retina layer thinning, photoreceptor disorganization, and swelling of inner segments as well as photoreceptor degeneration that are typical for late stages in AMD and RP. Changing the diet to a low-glycemic-index diet arrested the development of retinal degeneration, supporting a direct link between retinal degeneration, the microbiome, and its metabolites[54].

Most recently, Peng et al. reported that loss-of-function mutations in the *Crumbs homolog 1 (CRB1)* gene compromise both retinal and colonic epithelial barriers, with gut bacteria causing secondary retinal degeneration[55]. The RCS rats carry a frameshift mutation in the *MerTK* gene[26]. In addition to its key role in mediating the phagocytosis of POS by the RPE cells, *MERTK* is expressed in macrophages, where it plays a crucial role in reducing innate immune responses and promoting the clearance of apoptotic cells by efferocytosis[56]. Whether raising the rats under SPF conditions ameliorated innate responses in these rats remains to be determined.

Several gut microbial families found to be associated in our study with retinal degeneration were previously reported to be associated with neurodegenerative pathologies in the eye and brain[57]. For example, Clostridia Clostridiales (ASV number 09046, and ASV sequence can be found in Database S3) showed reduced abundance in RCS with high structural damage to the retina, as determined by BL-FAF (Fig. 5A). Another Clostridia Clostridiales (ASV number 10195) showed reduced abundance with reduced photoreceptor function as measured by delayed dark-adapted ERG b wave implicit time (Fig. 5C). While Clostridia Clostridiales taxa were shown to be increased in Neuromyelitis Optica (NMO) patients[58], they were shown to decrease in Parkinson's disease (PD) patients[57,59]. Ruminococcaceae Oscillospira (ASV12750) was found here to be reduced in RCS with large hypofluorescent BL-FAF areas (Fig. 5A). In contrast, taxa from the Ruminococcaceae family were found to be increased in PD patients, and this family is associated with disease progression[17,60]. Rowan et al. demonstrated the association between changes in gut microbiota and AMD-like retinopathy in mice fed a high glycemic diet[54,61]. Microbial taxa from the Clostridia family and Ruminococcaceae family were found to be associated with fundus damage[54]. Additionally, retinal neuroprotection was associated with increased levels of Akkermansia [54], which was not detected as different in our model. Prevotella copri, found here to be negatively associated with increased structural damage to the retina, as assessed by BL-FAF (Fig. 5A), was found in decreased levels in patients with PD[62]. This reduction was documented also in Amyotrophic Lateral Sclerosis[63], Multiple Sclerosis[64], and NMO[58]. These data suggest some commonality between changes in microbiome taxa and neurodegeneration in the retina and brain. However, mechanistic data regarding their potential impact on neurodegeneration remains limited and necessitates further research.

Our work has several strengths and some limitations. We reared RCS rats in an SPF environment and compared their microbiome composition and diversity, as well as retinal degeneration stage, to RCS rats that were bred in conventional conditions, with significant findings linking more rapid retinal deterioration in genetically susceptible RCS rats in non-SPF conditions that are also linked with different microbial composition. Rearing conditions were identical in both SPF and non-SPF facilities, including cages, bedding material, water, food, and light conditions. These similarities ensured that the differences in retinal degeneration patterns between the groups could not be attributed to variations in these environmental factors. Nevertheless, there may have been other differences between the housing facilities that we are unaware of. Other study limitations include using SPF conditions that allow the growth of non-pathogenic bacteria. It will be valuable to study further the effect of germ-free conditions on the retinal degeneration rate in these rats. In addition, we saw that litter was a significant factor linked with microbial composition. Still, since rats were born and reared in different housing conditions for two generations, no separation between animals from the same litter was done, as litter mixing would have resulted in switching from non-SPF to SPF conditions, which was not a feasible option. However, the number of rats ranged between four and eleven in each litter group, while the number of litters ranged from one to five in each group and age. In addition, we could control for litter in our multivariate analyses linking microbial ASVs to retinal structure and function. It is also possible that this study could have benefited from a larger number of animals.

In conclusion, RP is a blinding disease caused by dysfunction and degeneration of retinal photoreceptor cells. The disease is highly heterogeneous genetically, but even in patients with mutations in the same gene and in the same gene region, disease course and time of onset may vary considerably[3]. Furthermore, the patient's age, sex, baseline retinal function, and affected gene region accounted for less than a third of the variation in rates of change in retinal function[4]. These findings strongly suggest that factor(s) other than the gene defect itself may affect the clinical course of RP, suggesting genetic-environmental interaction affecting the disease course, potentially through the gut-eye axis. Here, in a genetic rat model of RP, we were able to show that different environment (SPF vs. non-SPF) affects the rate of retinal degeneration, and this was linked with alteration in the gut microbiome that is known to be related and affected by environmental factors more than by genetics. More mechanistic studies are needed to elaborate on the role of gut microbial composition in retinal degeneration. Identifying gut microbiota as potential contributing factors to retinal neurodegeneration in RP may lead to discovering novel therapeutic approaches to control or limit disease progression.

Methods

Animals and housing conditions

All animal procedures and experiments were conducted under the supervision of the Institutional Animal Care Committee at the Sheba Medical Center, Tel-Hashomer, and conformed with the recommendations of the Association for Research in Vision and Ophthalmology Statement for the Use of Animals in Ophthalmic and Vision Research. This study is reported in accordance with ARRIVE guidelines. Pigmented RCS rats and the WT Long Evans ("WT") rats were used in this study. In the SPF group, rats were bred, born, and raised in individually ventilated cages at the Sheba Medical Center SPF animal facility. The light conditions were similar in the SPF and non-SPF facilities, including the type of light source (fluorescent lamps) and the distance of the cages from the light source. Rats were born and reared in identical orange cages, which block the short wave length (Supplementary Fig. 10). Cages were of the same type and size in both facilities. In the SPF facility, the cages were closed and connected to a filtered air system. In the non-SPF facility, the cages were open to room air but covered from above with the same dark grey filter vent cage top to ensure identical light conditions inside the cages. Light intensity measured inside the cages was 2–4 lx in both facilities.

The Sheba SPF animal facility is registered and approved by the Israeli Ministry of Health. Entry is restricted to SPF-trained personnel only. Mandatory personal protective equipment includes room-dedicated shoes, scrubs, a face mask, hair bonnets, a room-dedicated gown, and gloves. All materials (cages, bedding, nesting material, feed, water bottles, enrichment material) are autoclaved before use. In the non-SPF group, rats were bred, born, and raised in open cages in the Goldschleger Eye Institute non-SPF animal facility under identical light, temperature, water, and feeding conditions. The non-SPF facility is a controlled, health-monitored environment. Rats were bred, born, and raised for at least two generations in each facility before the experiments. A similar number of males and females was included in each group and at each time point ($p = 0.081$). The rats tested in each group and of different ages were taken from two to five different litters, except for the age of 16 weeks, in which a single litter was used in the SPF and non-SPF conditions. For all procedures requiring anesthesia, rats were anesthetized with a mixture of xylazine and ketamine, as detailed in the relevant sections.

Blue auto fluorescence fundus (BL-FAF) imaging

BL-FAF imaging was performed using Spectralis SD-OCT (Heidelberg Engineering, Germany)[29]. Briefly, rats were anesthetized with an intraperitoneal injection of xylazine (10mg/kg; Eurovet Animal Health, Bladel, The Netherlands) and ketamine (75mg/kg; Vetoquinol, Lure, France) mixture. The optic disc and the blood vessels were used as an alignment target in the infrared (IR) scan mode. Then, the platform was switched to BL-FAF scanning mode, and the focus was adjusted for maximum clarity of the vessels. When a clear picture was obtained, the light setting was adjusted manually to eliminate overexposure as much as possible without losing the contour of blood vessels. BL-FAF images were taken in the superior and inferior regions relative to the optic nerve head (ONH) positioned at the screen's lower or upper part, respectively (Supplementary Fig. 11A). The Region Finder tool (version 26.2.0; Heidelberg Engineering) was used to assess the hypofluorescent area above and below the ONH. All scans were measured while applying preset picture parameters (shadow correction-9 pixels; smooth-3 pixels), minimal small vessel detection threshold (10 μm), maximum large vessel detection threshold (200 μm), and maximum bootstrap settings (98%). Block lines were used to block out blood vessels when automatic settings were insufficient and to block the ONH. The percentage of hypofluorescent area in each image was calculated from the total scanned area below or above the ONH center, defined as 100% (Supplementary Fig. 11B, C). Data are presented as the mean of both eyes and the results obtained by two masked readers (HKK and RS).

Spectral domain optical coherence tomography (SD-OCT)

Rats were anesthetized with an intraperitoneal injection of xylazine (10mg/kg; Eurovet Animal Health, Bladel, The Netherlands) and ketamine (75mg/kg; Vetoquinol, Lure, France) mixture. Both eyes were scanned with Spectralis SD-OCT (Heidelberg Engineering, Germany)[29]. Measurements of retinal layer thicknesses were taken from an area of 1.4- to 2.4 mm around the ONH (Supplementary Fig. 12). As previously described, SD-OCT scans were exported from the device as AVI files and analyzed using *ImageJ* (Fiji) version 1.51a[29]. Total retina (TR) thickness was measured from the inner limiting membrane to the RPE. The outer nuclear layer (ONL), which consists of the photoreceptor nuclei/cell bodies, was measured from the outer limiting membrane (OLM) to the INL/outer plexiform layer (OPL) interface. The debris zone (DZ), a hyperreflective layer, was observed and measured only in RCS rats (from the OPL to the RPE)[29]. For each eye, these measurements were averaged from four quadrants: Superior (SUP) and Mid-Superior (MID-SUP), Inferior (INF), and Mid-Inferior (MID-INF) to the ONH (Supplementary Fig. 12), and then both eyes were averaged using our published protocol[29].

Electroretinography (ERG)

Rats were kept in darkness for 12 h before ERG testing. Rats were anesthetized with an intraperitoneal injection of xylazine (10mg/kg; Eurovet Animal Health, Bladel, The Netherlands) and ketamine (75mg/kg; Vetoquinol, Lure, France) mixture e. Eyes were numbed with 0.4% oxybuprocaine hydrochloride eye drops (Localin; Fischer Pharmaceutical Laboratories Ltd., Tel Aviv, Israel), and pupils were dilated with a 0.5% tropicamide solution (Midramid; Fischer Pharmaceutical Laboratories Ltd.). The corneas were kept moist with topical 2.5% Hydroxypropyl methylcellulose. ERG responses were recorded from both eyes simultaneously using golden wire loops around the sclera, and a reference electrode was placed on the cornea. A ground electrode was placed on the rat's tail. For dark-adapted ERG, stimulus light intensities were 0.023, 0.249, 2.44, 4.4, and 23.5 cd-s/m^2, and responses were averaged with stimulus intervals of 1 to 30 s. For light-adapted ERG, the rats were light-adapted for 5 min before testing. Stimulus light intensities were: 0.249, 0.957, 2.44, 4.4, and 23.5 cd-s/m^2. In each animal at each

time point, the mean amplitude of the ERG recorded from both eyes was calculated for each light intensity[43]. The ERG a- and b-wave implicit time was measured from light onset to the first minimum (a-wave peak) and first positive (b-wave) peak.

Immunofluorescence analysis for S- and M/L-opsin

Paraffin blocks were prepared from enucleated eyes after euthanasia. 4-µm sections were cut along the vertical meridian of the eye through the optic nerve. Retinal cross sections were de-paraffinized by incubating in xylene and ethanol solutions at decreasing concentrations, as previously described[43,65]. For antigen retrieval, sections were incubated in 0.1M citrate buffer for 16 h at 70 degrees, followed by three washes with PBS for five minutes. Nonspecific antibody binding was blocked by incubating the sections in 5% BSA followed by 16-h incubation with primary antibodies (Rabbit anti-S opsin and Rabbit anti-M/L opsin polyclonal from Millipore) diluted 1:150 in 1% BSA at 4^0C, as previously described[66]. Following extensive washes in PBS, the sections were incubated with FITC-AffiniPure Goat Anti-Rabbit IgG (Jackson ImmunoResearch) diluted 1:150 in 1% BSA/PBS for one hour at room temperature. Sections were washed with PBS and mounted with mounting media containing 4,6-diamidino-2-phenylindole (DAPI, Bar-Naor, Israel). Sections were imaged using a fluorescent microscope (BX51, Olympus).

Apoptosis analysis

TUNEL staining was performed following manufacturer instructions (In Situ Cell Death Detection Kit, TMR red, Roche), as previously described[67]. Briefly, following rehydration, sections were incubated in permeabilization solution (0.1% Triton X-100, 0.1% sodium citrate) for two minutes on ice, followed by incubation with the TUNEL reaction mixture for 1 h at 37°C. The number of TUNEL-positive nuclei in the ONL was determined across entire retinal sections using *ImageJ* (Fiji) version 1.51a by three masked readers (IS, SD, GA). Results are presented as a mean number of TUNEL-positive nuclei in the ONL per 100 µm retina.

Fecal sample handling, DNA extraction, and 16S amplicon sequencing

Fresh fecal samples were collected with a sterile swab. Samples were stored at -80 °C until further processing. DNA extraction and PCR amplification of the variable region 4 (V4) of the 16S rRNA gene using Illumina adapted universal primers 515 F/806R 39 was conducted using the direct PCR protocol [Extract-N-Amp Plant PCR kit (Sigma-Aldrich)] as previously described[68–70]. Sequencing was performed on the Illumina MiSeq platform.

Microbiome data processing and analysis

Reads were processed in a data curation pipeline implemented in QIIME 2 version 2019.4[71,72] barcodes. Quality control was performed by truncating reads after three consecutive Phred scores lower than 20. Reads with ambiguous base calls or shorter than 150 bp after quality truncation were discarded. Sequence variants (SV) detection was performed using Deblur[73]. Reads were then truncated to 150 bp. The taxonomic classification of ASVs was performed using a naive Bayes fitted classifier, trained on the August 2013 99% identity Greengenes database. Unweighted UniFrac was used as a measure of β-diversity = between sample diversity. To avoid the sample size effect, all samples were rarefied to 2000 reads for β diversity analysis. The resulting distance matrix was used to perform a principal coordinate analysis (PCoA). A heatmap was generated using Calour version 2019.5.1 with default parameters[74]. Quantifications of variance were calculated using PERMANOVA in the R package Vegan_ENREF_42 on the rarefied Unweighted UniFrac distance values. The total variance explained by each variable was calculated while accounting for age in the model (except for when looking at the contribution of age and sex). MaAsLin2 (Multivariate Association with Linear Models) R package version 1.4.0[75] was used with default parameters to find ASVs significantly associated with BL-FAF hypofluorescent area > 10%, and ERG dark-adapted b-wave implicit time while controlling for litter, sex, age, and housing conditions (SPF vs. non-SPF). To control the effect of outliers, ASVs with expression in less than three samples within a category considered "high" were removed.

Statistical analysis

ANOVA followed by t-test paired analysis was performed to evaluate the effect of housing conditions at each time point on body weight, animals' sex, ERG, SD-OCT, BL-FAF, immunofluorescence imaging, and cell apoptosis. The Kruskal–Wallis test was used to evaluate these differences if the data was not normally distributed. For statistical analysis, ERG a-wave amplitudes ≤ 3 µV and b-wave amplitudes ≤ 5 µV were considered unmeasurable responses (amplitude = 0 µV). All analyses were performed using GraphPad Prism 8. Differences were considered significant if $p < 0.05$.

Data availability

The datasets generated and analyzed during the current study are available from the corresponding author upon reasonable request.

Received: 7 April 2024; Accepted: 22 August 2024
Published online: 16 September 2024

References

1. Hartong, D. T., Berson, E. L. & Dryja, T. P. Retinitis pigmentosa. *The Lancet* **368**, 1795–1809 (2006).
2. Bravo-Gil, N. *et al.* Unravelling the genetic basis of simplex retinitis pigmentosa cases. *Sci. Rep.* **7**, 41937 (2017).
3. Hamel, C. Retinitis pigmentosa. *Orphanet J. Rare Dis.* **1**, 40 (2006).

4. Berson, E. L., Rosner, B., Weigel-DiFranco, C., Dryja, T. P. & Sandberg, M. A. Disease progression in patients with dominant retinitis pigmentosa and rhodopsin mutations. *Invest. Ophthalmol. Vis. Sci.* **43**, 3027–3036 (2002).
5. Berson, E. L., Weigel-DiFranco, C., Rosner, B., Gaudio, A. R. & Sandberg, M. A. Association of vitamin A supplementation with disease course in children with retinitis pigmentosa. *JAMA Ophthalmol.* **136**, 490–495 (2018).
6. Berson, E. L., Rosner, B., Sandberg, M. A., Weigel-DiFranco, C. & Willett, W. C. ω-3 intake and visual acuity in patients with retinitis pigmentosa receiving vitamin A. *Arch. Ophthalmol.* **130**, 707–711 (2012).
7. Group, A.-R. E. D. S. R. A randomized, placebo-controlled, clinical trial of high-dose supplementation with vitamins C and E, beta carotene, and zinc for age-related macular degeneration and vision loss: AREDS report no. 8. *Arch. Ophthalmol.* **119**, 1417–1436 (2001).
8. Rotenstreich, Y. *et al.* Treatment with 9-cis β-carotene-rich powder in patients with retinitis pigmentosa: A randomized crossover trial. *JAMA Ophthalmol.* **131**, 985–992 (2013).
9. Ogunrinola, G. A., Oyewale, J. O., Oshamika, O. O. & Olasehinde, G. I. The human microbiome and its impacts on health. *Int. J. Microbiol.* **2020**, 8045646 (2020).
10. Turnbaugh, P. J. *et al.* An obesity-associated gut microbiome with increased capacity for energy harvest. *Nature* **444**, 1027–1031 (2006).
11. Yatsunenko, T. *et al.* Human gut microbiome viewed across age and geography. *Nature* **486**, 222–227 (2012).
12. Rodríguez, J. M. *et al.* The composition of the gut microbiota throughout life, with an emphasis on early life. *Microb. Ecol. Health Dis.* **26**, 26050 (2015).
13. Yassour, M. *et al.* Natural history of the infant gut microbiome and impact of antibiotic treatment on bacterial strain diversity and stability. *Sci. Transl. Med.* **8**, 343ra81 (2016).
14. Rothschild, D. *et al.* Environment dominates over host genetics in shaping human gut microbiota. *Nature* **555**, 210–215 (2018).
15. Turnbaugh, P. J. *et al.* The human microbiome project. *Nature* **449**, 804–810 (2007).
16. Erny, D. *et al.* Host microbiota constantly control maturation and function of microglia in the CNS. *Nat. Neurosci.* **18**, 965–977 (2015).
17. Scheperjans, F. *et al.* Gut microbiota are related to Parkinson's disease and clinical phenotype. *Mov. Disord.* **30**, 350–358 (2015).
18. Sampson, T. R. *et al.* Gut microbiota regulate motor deficits and neuroinflammation in a model of Parkinson's disease. *Cell* **167**, 1469-1480 e12 (2016).
19. Minter, M. R. *et al.* Antibiotic-induced perturbations in gut microbial diversity influences neuro-inflammation and amyloidosis in a murine model of Alzheimer's disease. *Sci. Rep.* **6**, 30028 (2016).
20. Andriessen, E. M. *et al.* Gut microbiota influences pathological angiogenesis in obesity-driven choroidal neovascularization. *EMBO Mol. Med.* **8**, 1366–1379 (2016).
21. Zinkernagel, M. S. *et al.* Association of the intestinal microbiome with the development of neovascular age-related macular degeneration. *Sci. Rep.* **7**, 40826 (2017).
22. Beura, L. K. *et al.* Normalizing the environment recapitulates adult human immune traits in laboratory mice. *Nature* **532**, 512–516 (2016).
23. Lane-Petter, W. Provision of pathogen-free animals. *Proc. R. Soc. Med.* **55**, 253–256 (1962).
24. Letson, H. L., Morris, J., Biros, E. & Dobson, G. P. Conventional and specific-pathogen free rats respond differently to anesthesia and surgical trauma. *Sci. Rep.* **9**, 9399 (2019).
25. Masri, S. & Sassone-Corsi, P. The emerging link between cancer, metabolism, and circadian rhythms. *Nat. Med.* **24**, 1795–1803 (2018).
26. D'Cruz, P. M. *et al.* Mutation of the receptor tyrosine kinase gene Mertk in the retinal dystrophic RCS rat. *Hum. Mol. Genet.* **9**, 645–651 (2000).
27. LaVail, M. M., Pinto, L. H. & Yasumura, D. The interphotoreceptor matrix in rats with inherited retinal dystrophy. *Invest. Ophthalmol. Vis. Sci.* **21**, 658–668 (1981).
28. Machida, S., Raz-Prag, D., Fariss, R. N., Sieving, P. A. & Bush, R. A. Photopic ERG negative response from amacrine cell signaling in RCS rat retinal degeneration. *Invest. Ophthalmol. Vis. Sci.* **49**, 442–452 (2008).
29. Bubis, E. *et al.* Blue autofluorescence fundus imaging for monitoring retinal degeneration in Royal college of surgeons rats. *Transl. Vis. Sci. Technol.* **8** (2019)
30. Ryals, R. C. *et al.* Long-term characterization of retinal degeneration in royal college of surgeons rats using spectral-domain optical coherence tomography. *Invest. Ophthalmol. Vis. Sci.* **58**, 1378–1386 (2017).
31. Bourne, M. C., Campbell, D. A. & Tansley, K. Hereditary degeneration of the rat retina. *Br. J. Ophthalmol.* **22**, 613–623 (1938).
32. Tso, M. O. *et al.* apoptosis leads to photoreceptor degeneration in inherited retinal dystrophy of RCS rats. *Invest. Ophthalmol. Vis. Sci.* **35**(6), 2693–2699 (1994).
33. Di Pierdomenico, J. *et al.* Early events in retinal degeneration caused by rhodopsin mutation or pigment epithelium malfunction: Differences and similarities. *Front. Neuroanat.* **11**, 14 (2017).
34. Campagnoli, L. I. M., Varesi, A., Barbieri, A., Marchesi, N. & Pascale, A. Targeting the gut-eye axis: An emerging strategy to face ocular diseases. *Int. J. Mol. Sci.* **24**, 13338 (2023).
35. Marmor, M. F. The electroretinogram in retinitis pigmentosa. *Archiv. Ophthalmol.* **97**, 1300–1304 (1979).
36. Wen, Y., Klein, M., Hood, D. C. & Birch, D. G. Relationships among multifocal electroretinogram amplitude, visual field sensitivity, and SD-OCT receptor layer thicknesses in patients with retinitis pigmentosa. *Invest Ophthalmol. Vis. Sci.* **53**, 833–840 (2012).
37. Sugita, T., Kondo, M., Piao, C.-H., Ito, Y. & Terasaki, H. Correlation between macular volume and focal macular electroretinogram in patients with retinitis pigmentosa. *Invest Ophthalmol. Vis. Sci.* **49**, 3551–3558 (2008).
38. Miller, R. F. & Dowling, J. E. Intracellular responses of the Müller (glial) cells of mudpuppy retina: Their relation to b-wave of the electroretinogram. *J. Neurophysiol.* **33**, 323–341 (1970).
39. Dolan, F. M., Parks, S., Hammer, H. & Keating, D. The wide field multifocal electroretinogram reveals retinal dysfunction in early retinitis pigmentosa. *Br. J. Ophthalmol.* **86**, 480–481 (2002).
40. Ohzeki, T., Machida, S., Takahashi, T., Ohtaka, K. & Kurosaka, D. The effect of intravitreal N-methyl-DL-aspartic acid on the electroretinogram in royal college of surgeons rats. *Jpn. J. Ophthalmol.* **51**, 165–174 (2007).
41. Fulton, A. B. Background adaptation in RCS rats. *Invest Ophthalmol. Vis. Sci.* **24**, 72–76 (1983).
42. Ciavatta, V. T., Mocko, J. A., Kim, M. K. & Pardue, M. T. Subretinal electrical stimulation preserves inner retinal function in RCS rat retina. *Mol. Vis.* **19**, 995–1005 (2013).
43. Tzameret, A. *et al.* Transplantation of human bone marrow mesenchymal stem cells as a thin subretinal layer ameliorates retinal degeneration in a rat model of retinal dystrophy. *Exp. Eye Res.* **118**, 135–144 (2014).
44. Bubis, E. *et al.* Blue autofluorescence fundus imaging for monitoring retinal degeneration in royal college of surgeons rats. *Transl. Vis. Sci. Technol.* **8**, 26 (2019).
45. Perlman, I. Dark-adaptation in abnormal (RCS) rats studied electroretinographically. *J. Physiol.* **278**, 161–175 (1978).
46. May, C. A., Horneber, M. & Lütjen-Drecoll, E. Quantitative and morphological changes of the choroid vasculature in RCS rats and their congenic controls. *Exp. Eye Res.* **63**, 75–84 (1996).
47. Tzameret, A. *et al.* Epiretinal transplantation of human bone marrow mesenchymal stem cells rescues retinal and vision function in a rat model of retinal degeneration. *Stem. Cell Res.* **15**, 387–394 (2015).

48. Tso, M. O. *et al.* Apoptosis leads to photoreceptor degeneration in inherited retinal dystrophy of RCS rats. *Invest. Ophthalmol. Vis. Sci.* **35**, 2693–2699 (1994).
49. Kutsyr, O. *et al.* Retinitis pigmentosa is associated with shifts in the gut microbiome. *Sci. Rep.* **11**, 6692 (2021).
50. Kutsyr, O. *et al.* Gradual increase in environmental light intensity induces oxidative stress and inflammation and accelerates retinal neurodegeneration. *Invest. Ophthalmol. Vis. Sci.* **61**, 1 (2020).
51. Polla, D. *et al.* A pilot study to evaluate the oral microbiome and dental health in primary open-angle glaucoma. *J. Glaucoma* **26**, 320–327 (2017).
52. Astafurov, K. *et al.* Oral microbiome link to neurodegeneration in glaucoma. *PLoS One* **9**, e104416 (2014).
53. Sun, M.-F. *et al.* Neuroprotective effects of fecal microbiota transplantation on MPTP-induced Parkinson's disease mice: Gut microbiota, glial reaction and TLR4/TNF-α signaling pathway. *Brain Behav. Immun.* **70**, 48–60 (2018).
54. Rowan, S. *et al.* Manipulation of gut microbiota affects diet- and age-related retinal degeneration. *Invest. Ophthalmol. Vis. Sci.* (2021).
55. Peng, S. *et al.* CRB1-associated retinal degeneration is dependent on bacterial translocation from the gut. *Cell* **187**, 1387-1401.e13 (2024).
56. Lemke, G. & Burstyn-Cohen, T. TAM receptors and the clearance of apoptotic cells. *Ann. N Y Acad. Sci.* **1209**, 23–29 (2010).
57. Gerhardt, S. & Mohajeri, M. H. Changes of colonic bacterial composition in Parkinson's disease and other neurodegenerative diseases. *Nutrients* **10**, 708 (2018).
58. Varrin-Doyer, M. *et al.* Aquaporin 4-specific T cells in neuromyelitis optica exhibit a Th17 bias and recognize Clostridium ABC transporter. *Ann. Neurol.* **72**, 53–64 (2012).
59. Hasegawa, S. *et al.* Intestinal Dysbiosis and lowered serum lipopolysaccharide-binding protein in Parkinson's disease. *PLoS One* **10**, e0142164 (2015).
60. Hill-Burns, E. M. *et al.* Parkinson's disease and Parkinson's disease medications have distinct signatures of the gut microbiome. *Mov. Disord.* **32**, 739–749 (2017).
61. Rowan, S. *et al.* Involvement of a gut-retina axis in protection against dietary glycemia-induced age-related macular degeneration. *Proc. Natl. Acad. Sci. U S A* **114**, E4472–E4481 (2017).
62. Petrov, V. A. *et al.* Analysis of gut microbiota in patients with Parkinson's disease. *Bull Exp. Biol. Med.* **162**, 734–737 (2017).
63. Brenner, D. *et al.* The fecal microbiome of ALS patients. *Neurobiol. Aging* **61**, 132–137 (2018).
64. Cantarel, B. L. *et al.* Gut microbiota in multiple sclerosis: Possible influence of immunomodulators. *J. Investig Med.* **63**, 729–734 (2015).
65. Edelshtain, V. *et al.* Long-term treatment with 9-cis-β-carotene rich alga *Dunaliella bardawil* ameliorates photoreceptor degeneration in a mouse model of retinoid cycle defect. *Algal. Res.* **43**, 101607 (2019).
66. Sher, I. *et al.* Synthetic 9-cis-beta-carotene inhibits photoreceptor degeneration in cultures of eye cups from rpe65rd12 mouse model of retinoid cycle defect. *Sci. Rep.* **8**, 6130 (2018).
67. Sher, I. *et al.* Repetitive magnetic stimulation protects corneal epithelium in a rabbit model of short-term exposure keratopathy. *Ocul. Surf.* **18**, 64–73 (2020).
68. Bier, A. *et al.* A high salt diet modulates the gut microbiota and short chain fatty acids production in a salt-sensitive hypertension rat model. *Nutrients* **10**, 1154 (2018).
69. Bier, A. *et al.* Antibiotic treatment does not ameliorate the metabolic changes in rats presenting dysbiosis after consuming a high fructose diet. *Nutrients* **12**, 203 (2020).
70. di Segni, A. *et al.* Guided protocol for fecal microbial characterization by 16S rRNA-amplicon sequencing. *J. Vis. Exp.* **133**, 56845 (2018).
71. Caporaso, J. G. *et al.* QIIME allows analysis of high-throughput community sequencing data. *Nat. Methods* **7**, 335–336 (2010).
72. Bolyen, E. *et al.* Reproducible, interactive, scalable and extensible microbiome data science using QIIME 2. *Nat. Biotechnol.* **37**, 852–857 (2019).
73. Amir, A. *et al.* Deblur rapidly resolves single-nucleotide community sequence patterns. *mSystems* **2**, e00191 (2017).
74. Xu, Z. Z. *et al.* Calour: An interactive, microbe-centric analysis tool. *mSystems* **4**, e00269 (2019).
75. Morgan, X. C. *et al.* Dysfunction of the intestinal microbiome in inflammatory bowel disease and treatment. *Genome Biol.* **13**, R79 (2012).

Author contributions

Conceptualization and experimental design: I.S., Y.H., Y.R.; Data collection and data analysis: H.K.K, R.S., I.S., G.A., S.D., Y.L.B, A.S., R.H., G.E., A.A., T. B., Y.H., Y.R.; Manuscript preparation: H.K.K, I.S., Y.H., Y.R. All authors reviewed the manuscript, approved the submitted version and have agreed both to be personally accountable for the author's own contributions and to ensure that questions related to the accuracy or integrity of any part of the work, even ones in which the author was not personally involved, are appropriately investigated, resolved, and the resolution documented in the literature.

Funding

This study was supported by the Israeli Ministry of Science, Technology, and Space (Grant Number: 3–15519, to YH and YR). IS is partially funded by The Nehemia Rubin Excellence in Biomedical Research, TELEM Program, Sheba Medical Center, Tel Hashomer, Israel.

Competing interests

The authors declare no competing interests.

Additional information

Supplementary Information The online version contains supplementary material available at https://doi.org/10.1038/s41598-024-70960-z.

Correspondence and requests for materials should be addressed to Y.H. or Y.R.